Surface pressure fluctuations produced by the total solar eclipse of 1 August 2008

Julien Marty, Francis Dalaudier, D. Ponceau, E. Blanc, U. Munkhuu

Surface Pressure Fluctuations Produced by the Total Solar Eclipse of 1 August 2008

J. MARTY*

CEA, DAM, DIF, Arpajon, France

F. DALAUDIER

CNRS/INSU, LATMOS/IPSL, Université Versailles St-Quentin, and UPMC-Paris 6, Paris, France

D. PONCEAU+ AND E. BLANC

CEA, DAM, DIF, Arpajon, France

U. MUNKHUU

RCAG, Ulaanbaatar, Mongolia

(Manuscript received 18 March 2012, in final form 4 October 2012)

ABSTRACT

During a solar eclipse, the moon's shadow progressively occults a part of Earth from the solar flux. This induces a cooling in the atmospheric layers that usually absorb the solar radiation. Since the eclipse shadow travels within the atmosphere at supersonic velocity, this cooling generates a planetary-scale bow wave of internal gravity waves. The purpose of this article is to estimate the surface atmospheric pressure fluctuations produced by the passage of the 1 August 2008 total solar eclipse and to compare these pressure fluctuations with those recorded by a temporary network of microbarographs and by the infrasound stations of the International Monitoring System. The surface pressure fluctuations expected at all the measurement sites are estimated using a linear spectral numerical model. It is shown that the cooling of both the ozonosphere and the troposphere can produce detectable pressure fluctuations at the ground surface but that the tropospheric cooling is likely to be the predominant source. Since the expected eclipse signals are in a frequency range that is highly perturbed by atmospheric tides and meteorological phenomena, the pressure fluctuations produced by these latter synoptic disturbances are characterized and removed from the recorded signals. Low-frequency gravity waves starting just after the passage of the eclipse are then brought to light at most measurement sites. The time–frequency characteristics of these waves are similar to those obtained from the model, which strongly suggests that these waves were produced by the passage of the 1 August 2008 solar eclipse.

1. Introduction

Molecular oxygen, ozone, and water vapor are the main gases responsible for the absorption of solar radiation within the atmosphere. During the day, these gases respectively heat the thermosphere, the stratosphere, and the troposphere. The thermal forcing produced by the daily heating of these absorption regions generates large-scale gravity waves at subharmonic periods of a solar day. These waves, called atmospheric solar tides, cause regular pressure oscillations that have been observed at Earth's surface for more than a century (Simpson 1918; Chapman and Westfold 1956; Dai and Wang 1999). During a total solar eclipse, the moon moves through the sun–Earth axis, progressively screening a part of the atmosphere from solar radiation. This induces a cooling in the part of the atmosphere occulted by the eclipse shadow. Since the eclipse shadow moves within the atmosphere at supersonic velocity, Chimonas (1970) showed that this atmospheric cooling

* Current affiliation: CTBTO, Vienna, Austria.
+ Current affiliation: CGGVeritas, Massy, France.

Corresponding author address: Julien Marty, CTBTO, P.O. Box 1200, 1400 Vienna, Austria.
E-mail: julien.marty@ctbto.org

DOI: 10.1175/JAS-D-12-091.1

could act as a continuous source of internal gravity waves and produce a planetary-scale bow wave. He estimated that the thermospheric cooling could not produce detectable waves at the ground surface because of the exponential decrease of the atmospheric density with the altitude. He then calculated that the stratospheric cooling could generate ground pressure fluctuations with amplitudes of 1 Pa, horizontal wavelengths of several thousands of kilometers, and periods around 10 h. The tropospheric cooling was not modeled because of the lack of knowledge on the shape and the altitude of the water vapor absorption region, but Chimonas (1970) mentioned that this cooling could produce waves with greater amplitudes than those produced by the cooling of the ozone layer.

Soon after this first modeling, Anderson et al. (1972) set up a measurement campaign to detect the ground pressure fluctuations produced by the passage of the 7 March 1970 total solar eclipse. They identified waves with an amplitude of 25 Pa and a central period of 90 min. Chimonas (1973) demonstrated that waves with such characteristics could not be induced by the global cooling of the ozonosphere. To explain these observations, he proposed a second theory based on the generation of Lamb waves from the radiative cooling of cloud layers. Two decades later, Fritts and Luo (1993) proposed an extension to Chimonas (1970) theory by numerically solving the pseudoincompressible perturbation equations in the eclipse shadow reference frame. They used the same stratospheric thermal forcing term and background atmospheric conditions as Chimonas (1970). They presented stationary solutions related to the middle and upper atmosphere but not to the ground surface. More recently, Eckermann et al. (2007) studied the response of the atmosphere to the passage of the total solar eclipse of 4 December 2002 using a prototype high-altitude global numerical weather prediction model. They estimated pressure fluctuations of several tens of pascals at ground level. These pressure fluctuations were explained by the cumulative effects of the stratospheric and tropospheric cooling as well as by the drop of temperature at Earth's surface, which was particularly intense over land.

Contrary to most gravity wave sources (orography, convection, geostrophic adjustment, etc.), the spatial and temporal evolution of the eclipse shadow can be easily and precisely determined a long time in advance. This is why several measurement campaigns were set up with the aim of detecting the ground pressure fluctuations produced by the passage of solar eclipses. Jones (1999) summarized that among all these attempts, most of them failed to detect such fluctuations (e.g., Schödel et al. 1973; Beckman and Clucas 1973; Anderson and Keefer 1975; Jones and Bogart 1975; Jones 1976, 1999) or gave ambiguous results (e.g., Venkatachari et al. 1982; Jones et al. 1992; Venkatachari et al. 1996). These nondetections might be due to the small amplitude of the expected waves, the simplicity of the existing models, or the short duration of the measurements, which prevents differentiating the waves produced by solar eclipses from those produced by other sources.

In a few cases only, authors provided evidence of a link between the detection of gravity waves and the passage of a solar eclipse. Among these observations, results are quite heterogeneous with 4-h-period waves of 10–15-Pa amplitude (Seykora et al. 1985), 23-min-period waves of 0.1–0.2-Pa amplitude (Goodwin and Hobson 1978), and 9–12-min-period waves of 3-Pa amplitude (Farges et al. 2003). The heterogeneity of these observations might be explained by the fact that the measurement campaigns were set up at different distances from the path of the total eclipse. The microbarograph network used by Seykora et al. (1985) was deployed at several thousands of kilometers from the central line of the eclipse whereas those used by Goodwin and Hobson (1978) and Farges et al. (2003) were only at a few hundreds of kilometers. Nevertheless, none of these detections can be clearly linked to any of the modeling proposed by either Chimonas (1970), Fritts and Luo (1993), or Eckermann et al. (2007). The period of the waves observed by Goodwin and Hobson (1978) and Farges et al. (2003) are for instance too short to have been produced by the global cooling of either the stratosphere or the troposphere. These waves could nevertheless result from the cooling of smaller-size absorption regions such as clouds or water vapor inhomogeneities. In summary, despite several modeling efforts and measurement campaigns, it is still unclear whether the cooling of the atmosphere during the passage of a solar eclipse can produce a planetary bow wave of internal gravity waves with large enough amplitude to be detected at Earth's surface.

The purpose of this paper is to estimate the surface atmospheric pressure fluctuations produced by the total solar eclipse of 1 August 2008 and to compare these pressure fluctuations with those recorded by a temporary network of microbarographs and the infrasound stations of International Monitoring System (IMS). To do so, we use the linear spectral numerical model described by Marty and Dalaudier (2010). This model was already used to study the cooling of the ozone layer during the passage of a total solar eclipse. Marty and Dalaudier (2010) showed that the asymptotic response to a Gaussian thermal forcing traveling at constant velocity was in good agreement with results obtained by Fritts and Luo (1993). They also obtained a stratospheric response similar at the first order to that presented by

Eckermann et al. (2007) for the 4 December 2002 solar eclipse. In section 2, we start by studying the pressure field produced at the ground surface by the passage of the 4 December 2002 solar eclipse in order to compare our results with Eckermann et al. (2007). It is shown that the cooling of the ozonosphere cannot explain the surface pressure perturbation obtained by Eckermann et al. (2007). We therefore consider a tropospheric cooling and show that this cooling is likely to be the predominant source of pressure perturbations produced at Earth's surface. The model is then used to study the case of the 1 August 2008 solar eclipse and estimate the ground pressure fluctuations produced at all the measurement sites by the cooling of the stratospheric and tropospheric regions.

In section 3, we describe a temporary network of microbarographs set up in western Mongolia to detect the waves produced by the 1 August 2008 total solar eclipse. Along with data from this temporary network, we also use the pressure measurements recorded by the permanent IMS infrasound network. This worldwide infrasound network is composed of 60 multicomponent stations of which 45 are already operationally certified. Although the IMS infrasound stations were designed to detect atmospheric pressure fluctuations produced by nuclear explosions in the 0.02–4-Hz-frequency range, Marty et al. (2010) recently demonstrated that the pressure measurements recorded by the majority of IMS infrasound stations are also accurate in the entire gravity wave–frequency range.

In section 4, we analyze the pressure measurements recorded by both the temporary microbarograph network and the closest IMS infrasound stations to the total eclipse path. Since the period of the expected pressure signals is in a band highly disturbed by atmospheric tides and meteorological processes, the pressure fluctuations produced by these synoptic disturbances are characterized and removed, as much as possible, from the recorded signals. Two low-frequency pressure signals starting just after the passage of the eclipse are then identified at stations of the temporary microbarograph network as well as at most of the closest IMS infrasound stations to the total eclipse path. The time–frequency characteristics of these two waves are similar to those produced from the model with the stratospheric and tropospheric sources, which shows that these two waves were likely produced by the passage of the 1 August 2008 total solar eclipse.

2. Modeling

a. Stratospheric and tropospheric sources

Eckermann et al. (2007) used a prototype high-altitude global numerical weather prediction model to study the response of the atmosphere to the total solar eclipse of 4 December 2002. They showed that a large-scale bow wave was produced in the middle atmosphere as well as in the troposphere. They obtained pressure fluctuations of several tens of pascals at ground level. To identify the main source responsible for these pressure fluctuations, we use the linear spectral numerical model described by Marty and Dalaudier (2010). This model was proposed to get first-order estimations of gravity wave fluctuations produced by sources with evolving sizes, trajectories, and velocities. It is based on the solutions of the linearized fundamental fluid equations (Fritts and Alexander 2003) and uses the fully compressible dispersion relation for inertia-gravity waves. Since this model can account for spatial and temporal variations of sources, Marty and Dalaudier (2010) already applied it to the case of the ozonosphere cooling during the passage of the 4 December 2002 solar eclipse. They found results in good agreement with those obtained by Eckermann et al. (2007) in the middle atmosphere. To study the pressure perturbation produced at Earth's surface, we start by applying the model to the same solar eclipse. Following Marty and Dalaudier (2010), we take into account the changes in shadow trajectory and velocity and consider the reflection of gravity waves at the ground surface. We also use the same thermal forcing term, atmospheric parameters, and eclipse characteristics.

Figure 1 represents the perturbation of the vertical velocity field at 80 km altitude (Fig. 1a) and the pressure field at the ground surface computed with the linear model (Fig. 1b). These two wave fields correspond to Figs. 13c and 15 presented by Eckermann et al. (2007). We can see that the bow wave observed at 80-km altitude is similar to the first order to the response obtained by Eckermann et al. (2007). The intensity of our wave field is slightly lower but it could be due to the fact that we consider a constant Gaussian daily heating rate profile (with an amplitude of 20 K day^{-1}) whereas Eckermann et al. (2007) used a spatially and temporally variable heating rate profile. On the contrary, the response obtained at ground level is very different from that presented by Eckermann et al. (2007). In the two solutions, we can see a large-scale bow wave but the amplitude of the pressure fluctuations produced with our model is at least one order of magnitude lower than that obtained by Eckermann et al. (2007). Moreover, the shape of the bow wave is clearly different. The amplitude of the pressure fluctuations obtained with our model is about 1.5 Pa, which is in agreement with the pressure fluctuations obtained by Chimonas (1970) for the cooling of the ozone layer. It therefore seems that the cooling of the ozonosphere can produce detectable

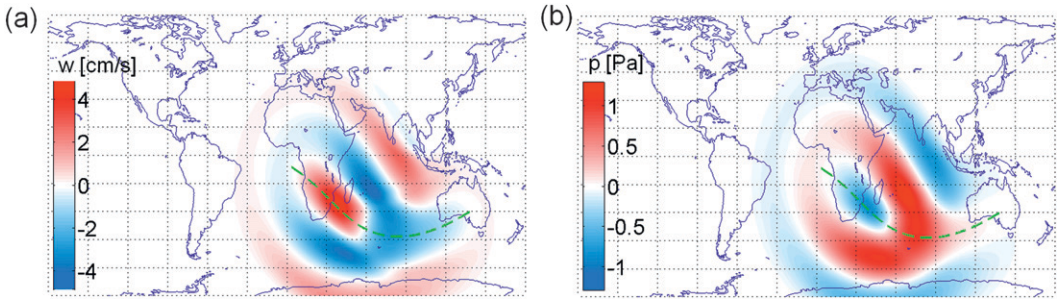

FIG. 1. Response of the atmosphere to the cooling of the ozone layer at 1000 UTC 4 Dec 2002 with (a) the vertical velocity wavefield at an altitude of 80 km and (b) the pressure wavefield at the ground surface. Scales and units are given in colorbars and the green dashed line shows the central line of the total eclipse path.

pressure fluctuations at the ground but that it is not the predominant source of the surface perturbation.

Since the model proposed by Marty and Dalaudier (2010) is linear, it can then be used to study independently the surface pressure fluctuations produced by different atmospheric thermal forcings. We therefore consider the cooling of the troposphere during the same solar eclipse. This cooling is due to the reduction of infrared absorption by water vapor. Water vapor is much more inhomogeneously distributed within the atmosphere than ozone. These inhomogeneities can produce local variations of the atmospheric cooling, which could generate smaller-scale waves compared to the dimension of the large-scale bow wave. Such inhomogeneities could be the source of the waves observed by Goodwin and Hobson (1978) or Farges et al. (2003). Despite the inhomogeneity of the water vapor distribution, we can see that Eckermann et al. (2007, their Fig. 15) obtained a clear large-scale bow wave at Earth's surface. This supports the idea of a global response of the troposphere. We therefore consider a vertical Gaussian distribution for the tropospheric absorption coefficient. The thermal forcing term is defined as

$$F_{\mathrm{Tn}}(x,y,z) = QE_{\mathrm{Ob}}(\mu_n)\exp\left[-\frac{(z-z_0)^2}{2\sigma_z^2}\right], \qquad (1)$$

with $z_0 = 3$ km, $\sigma_z = 1$ km, and $Q = -5$ K day^{-1}. The numerical values were chosen to approach a cooling characteristic of the troposphere (Eckermann et al. 2007, their Fig. 8). The function $\mu_n(x, y)$ is defined by Marty and Dalaudier (2010) to approximate the eclipse magnitude at the time t_n in the shadow region and E_{Ob} represents the eclipse obscuration—that is, the fraction of the surface area of the solar disk occulted by the moon (Espenak and Anderson 2001; Eckermann et al. 2007). Although solar intensity is brighter at the disk center than near the limb in the ultraviolet band, the solar irradiance is quasi uniform across the solar disk in the near infrared (Eckermann et al. 2007). Solar limb darkening effects can therefore be neglected when calculating the tropospheric thermal forcing term. As for the case of the ozone layer cooling, we take into account changes in shadow trajectory and velocity and also consider the reflection of gravity waves at the ground surface. We also use the same eclipse characteristics but consider atmospheric parameters related to the troposphere—that is, an atmospheric temperature $T = 290$ K, a buoyancy frequency $N = 0.01$ rad s^{-1}, and a density-scale height $H = 10$ km.

Figure 2 represents the pressure perturbation obtained at the ground surface at 1000 UTC. We can see that the shape of this wavefield is much more similar to that obtained by Eckermann et al. (2007) than the wavefield obtained from the cooling of the ozonosphere (Fig. 1b). We indeed retrieve the same high pressure region over the Indian Ocean and the south of Africa. The amplitude of the wavefield (from −5 to +12 Pa) is one order of magnitude higher than for the case of the ozone cooling but is still lower than that found by Eckermann et al. (2007) (from −16 to +53 Pa). This might be due to the fact that we did not take into account

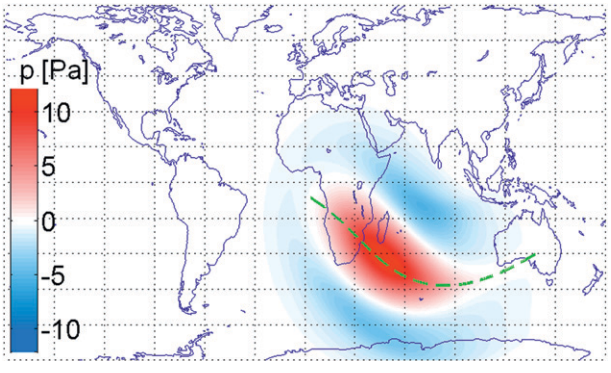

FIG. 2. Pressure wavefield produced at the ground surface by the cooling of the troposphere at 1000 UTC 4 Dec 2002. Scales and units are given in the colorbar and the green dashed line shows the central line of the total eclipse path.

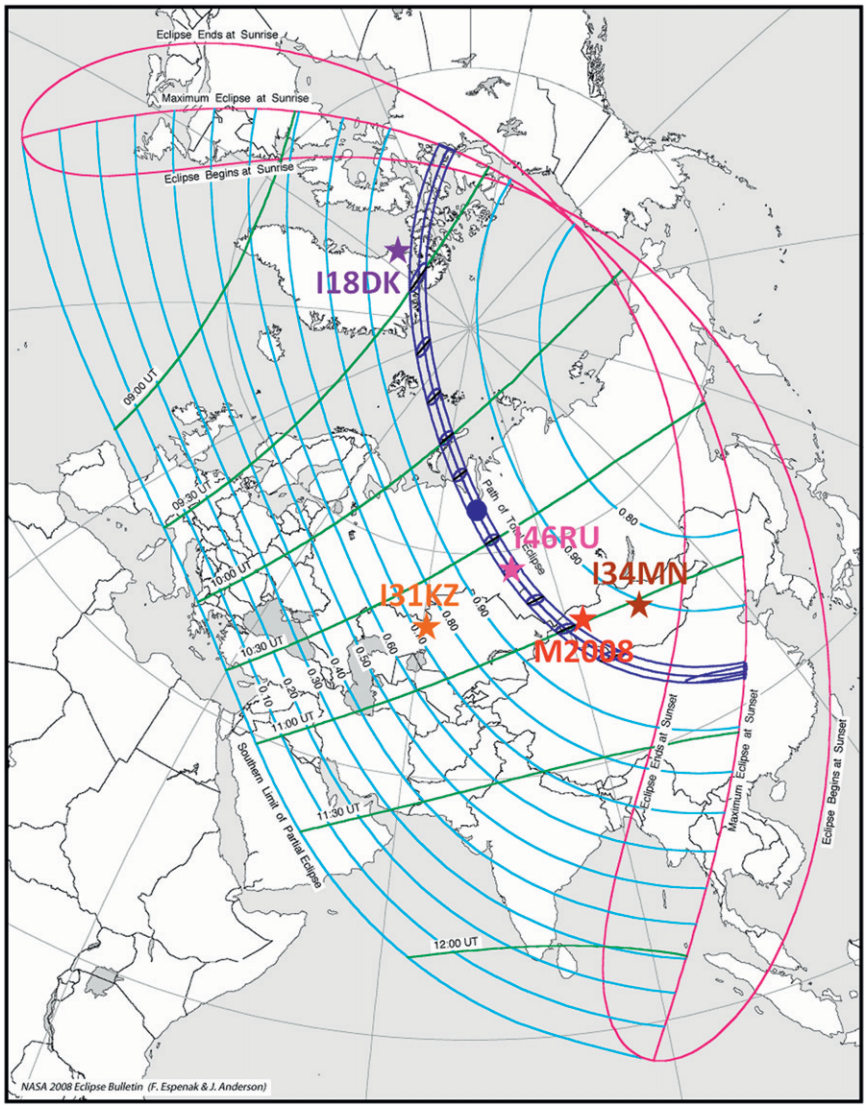

FIG. 3. Stereographic projection map of the eclipse (Espenak and Anderson 2007). The dark blue lines represent the limits and the center of the total eclipse path, the green lines the time (UTC) of the eclipse maximum, and the light blue lines the obscuration at the eclipse local maximum. The red star represents the location of the temporary microbarograph network deployed in western Mongolia (M2008) and the other colored stars are the locations of the four closest certified IMS infrasound stations to the total eclipse path. The blue disk represents the eclipse maximum.

the radiative effects of the cloud layers and of the ground surface (Eaton et al. 1997). In conclusion, this result shows that the cooling of the troposphere is more likely to produce detectable pressure fluctuations at Earth's surface than the cooling of the ozonosphere.

b. Solar eclipse of 1 August 2008

The solar eclipse of 1 August 2008 was the sixth total solar eclipse of the twenty-first century. It lasted about 2 h on Earth's surface. It started at 0924 UTC in Canada and then moved through Greenland, the northern Atlantic, Russia, Kazakhstan, and Mongolia (Fig. 3). It ended over northeastern China at 1118 UTC. The total eclipse reached its maximum in northern Russia with a maximum duration of 2 min 27 s in the center of the total eclipse path, a minimum velocity of 900 m s^{-1}, and a magnitude of 1.0185 (Espenak and Anderson 2007). The eclipse magnitude is defined as the fraction of the sun's diameter occulted by the moon. It is strictly a ratio of diameters and should not be confused with eclipse obscuration, which is a measure of the sun's surface area occulted by the moon (Espenak and Anderson 2007).

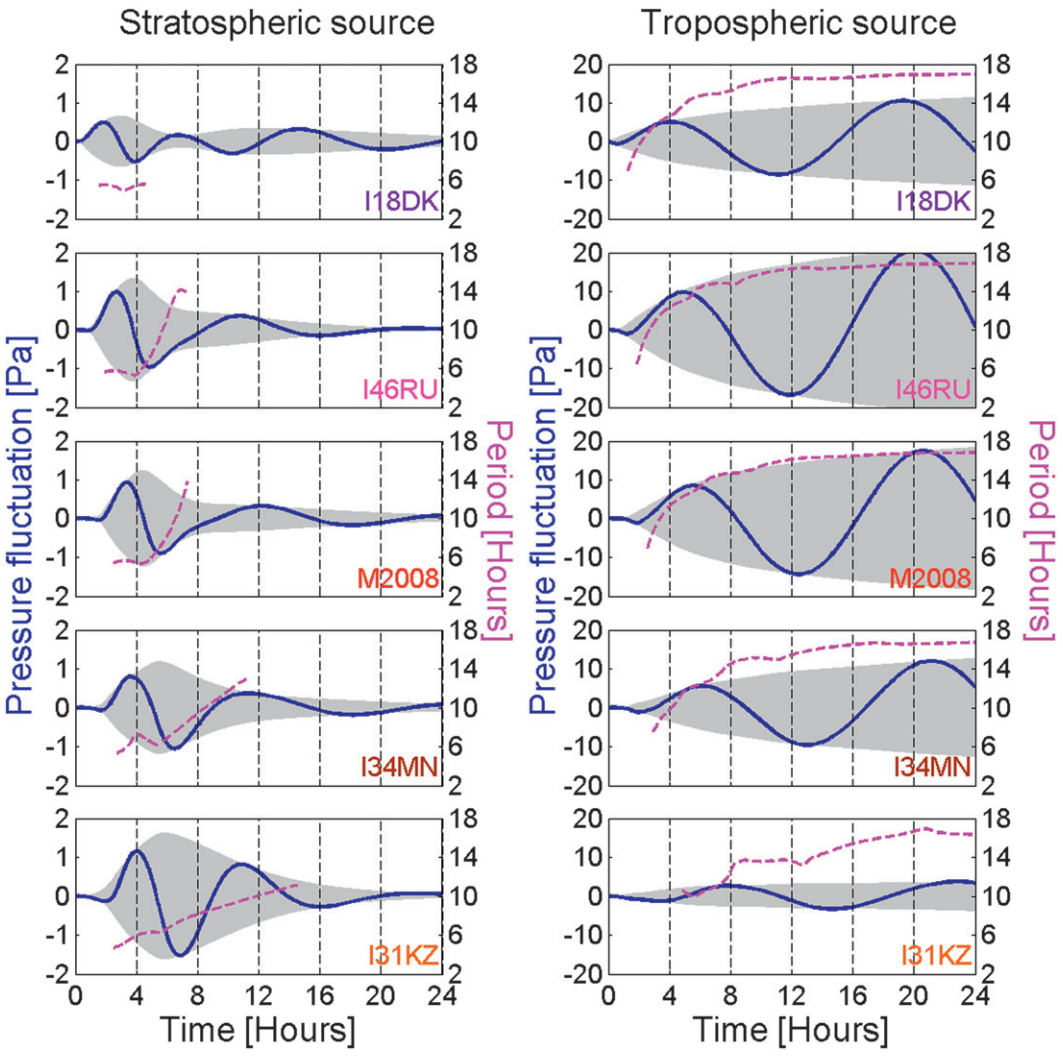

FIG. 4. Synthetic pressure fluctuation signals produced by the cooling of (left) the stratosphere and (right) the troposphere during the passage of the 1 Aug 2008 total solar eclipse at the position of the temporary network installed in western Mongolia (M2008) and at the position of the four closest certified IMS infrasound stations to the total eclipse path. The pressure fluctuation is plotted in solid blue, the period in dashed purple, and the signal envelope shaded in light gray.

The eclipse geometry depends on the relative orbital motions of Earth and the moon. During the 4 December 2002 total solar eclipse, the eclipse shadow moved through tropical regions and the entire penumbral region struck Earth's surface for most of the eclipse duration. The penumbral perimeter was therefore closed except during the beginning and end phases of the eclipse. Since the contribution of these two extreme phases to the total atmospheric cooling was low (Marty and Dalaudier 2010), we approximated the shape of the penumbral region by a disk of constant radius. The case of the 1 August 2008 total solar eclipse is different because the eclipse shadow moved through the North Pole region and the penumbral perimeter was continuously interrupted by the solar terminator (Fig. 3). It is therefore less accurate to approximate the penumbral region by a disk. However, since we look for the qualitative but not quantitative response to the 1 August 2008 total solar eclipse, we nevertheless keep this approximation, which simplifies the implementation of the model. For the same reason, the model is run for the same stratospheric and tropospheric forcing terms as those used in section 2a. The considered eclipse characteristics (trajectory, velocity, and magnitude) are those provided by Espenak and Anderson (2007).

Figure 4 presents the pressure signals (solid blue) produced by the stratospheric (left) and tropospheric (right) thermal forcings at the position of the temporary

microbarograph network M2008 installed in western Mongolia and at the position of the four IMS infrasound stations shown in Fig. 3. Note that all these stations will be further described in section 3. The instantaneous period of all pressure signals is plotted in dashed purple and the signal envelope in light gray. Since the complex wavefield obtained from the model corresponds to the complex conjugate of the analytic signal (Marty and Dalaudier 2010, their section 2b), the instantaneous period and the signal envelope were directly calculated from the time derivative of the wavefield phase. The period is not plotted when the signal envelope is too weak.

In Fig. 4, we can first see that the maximum amplitude of the pressure signals produced from the model with the stratospheric source is about 1.5 Pa, whereas it is about 20 Pa for the tropospheric source. The greatest intensity of the tropospheric response is in agreement with the discussion in section 2. It can also be seen that the amplitude of the pressure fluctuations produced by the stratospheric source is greater for the stations located farthest from the total eclipse path (I34MN, I31KZ), whereas that produced by the tropospheric source is higher for the closest stations (I46RU, M2008, I18DK). This is due to the fact that the wavelengths excited by the tropospheric forcing term propagate slower than those excited by the stratospheric forcing term. Thus, the maximum amplitude produced by the tropospheric forcing will arrive more than 24 h after the passage of the solar eclipse at the I31KZ and I34MN stations.

If we look at the pressure fluctuations produced by the stratospheric source and expected at the closest stations to the total eclipse path (M2008, I18DK, I46RU), we can see that the maximum amplitude is reached about 2–3 h after the passage of the total solar eclipse. At this time, the period of the signal is about 5 h. To our knowledge, Seykora et al. (1985) are the only ones who reported the observation of such low-frequency pressure fluctuations (4 h) at the ground surface after the passage of a solar eclipse. However, the amplitude of the ground pressure fluctuations they recorded was about 10–15 Pa, which seems incompatible with the cooling of the ozone layer. Contrary to the case of the stratospheric source, the maximum amplitude of the pressure signals produced by the tropospheric source is reached about 20 h after the passage of the solar eclipse (for the same three stations M2008, I18DK, and I46RU). The instantaneous period is about 8 h at the beginning. It then increases rapidly toward the inertia period, which is about 17 h 30 min for the chosen Coriolis parameter.

If we now look at the stations located farthest from the total eclipse path (I34MN and I31KZ), we can see that the maximum amplitude of the pressure signals produced by the stratospheric source arrives about 6–7 h after the passage of the total solar eclipse. The pressure fluctuations produced by the tropospheric source arrive almost at the same time and have similar amplitudes (about 3 Pa). The period of the stratospheric and tropospheric signals are however different, allowing these two pressure fluctuation signals to be distinguished.

As a conclusion, the pressure signals produced by the stratospheric and tropospheric sources have different waveforms and can be distinguished from one another. However, the amplitude of the pressure fluctuations produced by the stratospheric source is small compared to ambient pressure fluctuations. The pressure fluctuations produced by the tropospheric source can also be difficult to identify because of the energetic pressure fluctuations produced in the same period range by atmospheric tides and meteorological processes.

3. Mongolia 2008 measurement campaign

a. Network description

The modeling results presented in section 2 showed that the passage of the 1 August 2008 solar eclipse could generate a planetary bow wave and produce pressure fluctuations with periods from 4 to 17 h at Earth's surface. To characterize such a bow wave, the measurement sites must be located at thousands of kilometers from one another. This distance roughly corresponds to the average distance between the infrasound stations of the IMS infrasound network. This network consists of 60 worldwide-distributed stations, among which 45 are already operationally certified and continuously transmit data to the International Data Center in Vienna, Austria. The stations are miniarrays of infrasound sensors, which measure micropressure changes produced at ground level by infrasonic wave propagation. Although this network was designed to detect atmospheric pressure fluctuations produced by nuclear explosions in the 0.02–4-Hz-frequency range, Marty et al. (2010) recently demonstrated that the pressure measurements recorded by the majority of IMS infrasound stations are also accurate in the entire gravity wave–frequency range. They showed that the instrumental noise, the transfer function uncertainties, and the thermal susceptibility of the measuring chains do not significantly alter the pressure measurements in the gravity wave–frequency range. In Fig. 3, we can see that four certified IMS infrasound stations are located at less than 2000 km from the total eclipse path: I46RU (Russia, 65 km), I18DK (North Greenland, 220 km), I34MN (Mongolia, 990 km), and I31KZ (western Kazakhstan, 1650 km).

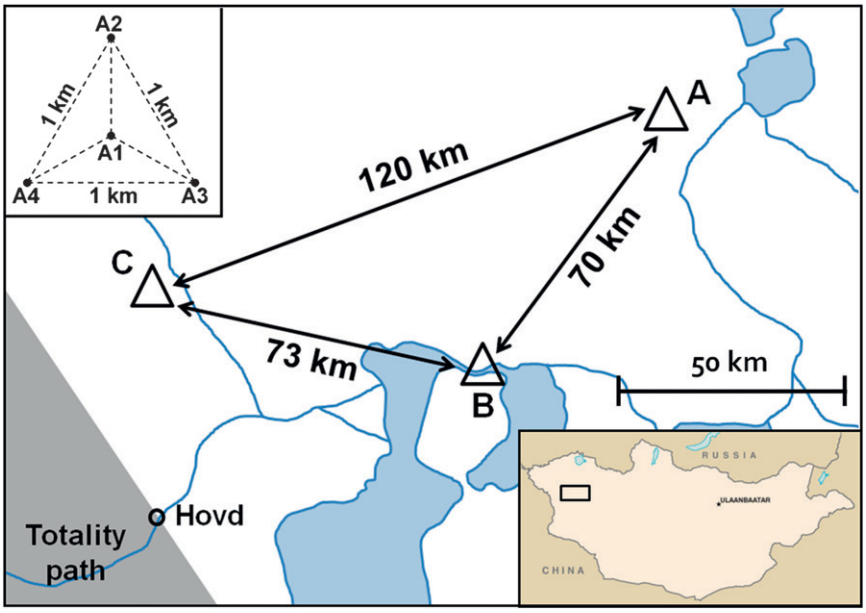

FIG. 5. Position of the three stations of the M2008 network. The total eclipse path is plotted in gray. The geometry of station A array elements is represented in the upper-left corner. Stations B and C have the same array element geometry as station A.

As discussed in the introduction, the majority of the measurement campaigns set up to detect ground pressure fluctuations produced by the passage of solar eclipses either failed to detect such fluctuations or gave ambiguous results (Jones 1999). Most of those who reported evidence of a link between the detection of gravity waves and the passage of a solar eclipse reported waves with periods from 10 to 90 min (Anderson et al. 1972; Goodwin and Hobson 1978; Farges et al. 2003). However, as discussed in section 2, these waves have periods that are too short to have been produced by the global cooling of either the troposphere or the stratosphere. These pressure fluctuations might nevertheless have been produced by smaller-size sources such as the cooling of water vapor inhomogeneities or clouds (Chimonas 1973). Since the IMS infrasound network can be used to study the bow wave produced by the passage of the 1 August 2008 solar eclipse, the French Atomic Energy Commission (CEA) decided to install a temporary microbarograph network that was adapted to the detection of short-period waves similar to those previously observed (Anderson et al. 1972; Goodwin and Hobson 1978; Farges et al. 2003). This network was installed in western Mongolia in the frame of the scientific collaboration between the CEA and the Research Center of Astronomy and Geophysics (RCAG) of the Mongolian Academy of Sciences.

The main objective of the Mongolia 2008 (M2008) temporary measurement campaign was to detect and analyze the gravity waves produced by the passage of the 1 August 2008 solar eclipse. To distinguish these waves from the waves produced by other sources, the microbarograph network was set up for 20 days around the passage of the solar eclipse. Three stations (or miniarrays) of four measurement points were installed 100 km apart from one another (Fig. 5). Such a distance was chosen for the characterization of a group velocity of about 320 m s^{-1}, similar to that observed by Goodwin and Hobson (1978) and Farges et al. (2003). The four measurement points of each station were positioned as described in the upper-left corner of Fig. 5. This geometry was chosen to optimize the calculation of phase velocities and azimuths of waves having horizontal wavelength longer than 500 m.

b. *Sensor description*

The microbarometers used during the M2008 measurement campaign were Martec MB2005 (CEA/DASE 1998). These sensors record pressure fluctuations from DC to tens of hertz including the entire gravity wave–frequency range. They are therefore adapted to the detection of the low-frequency pressure fluctuations estimated with the model (see section 2b) as well as to the detection of higher-frequency pressure fluctuations such as those previously observed after the passage of solar eclipses (Anderson et al. 1972; Goodwin and Hobson 1978; Farges et al. 2003). The pressure signals were recorded with a 20-Hz sampling frequency, which

prevents any temporal aliasing in the gravity wave–frequency band.

MB2005 microbarometers have a thermal susceptibility lower than 10 Pa K^{-1}, which is very low compared to other types of infrasound sensors such as microphones (Ponceau and Bosca 2010). Such a thermal susceptibility could however still produce significant fluctuations, especially at the diurnal period. Since this phenomenon was anticipated, all the measuring chains were installed underground (with air inlets at the surface) in order to reduce the amplitude of temperature changes in the sensor. A temperature sensor was also glued inside each microbarometer to record temperature changes within sensor measurement cavities. We will see in the next section that these temperature records along with a good estimation of each sensor thermal susceptibility allow an excellent correction of pressure signals from the influence of the temperature changes.

4. Data processing

a. *M2008 pressure measurements*

1) Correction from sensor thermal susceptibility

The objective of this section is to evaluate and remove the influence of temperature changes on the pressure measurements recorded during the M2008 measurement campaign. Figure 6 represents the power spectral density (PSD) of the raw pressure signal recorded by the B1 measuring chain during 21 days (blue curve). The two peaks observed on the PSD at diurnal and semidiurnal periods are produced by atmospheric tides and have been discussed by Marty et al. (2010). The PSD of the temperature recorded inside the sensor measurement cavity is represented in dashed orange and that recorded outside the station in dashed red. Comparing these two PSDs, we can see that the PSD of the temperature recorded inside the sensor is filtered out as the frequency increases. This is due to the fact that care was taken to ensure thermal insulation of the sensors by installing them underground. We can also observe that the PSD of the temperature recorded inside the sensor decreases faster than that of the pressure as the frequency increases. This shows that the more the frequency increases the less the thermal susceptibility will affect the pressure signal.

The thermal susceptibility of the B1 microbarometer as provided by the manufacturer is -2.8 Pa K^{-1}. The pressure PSD corresponding to the spurious fluctuations induced by this thermal susceptibility is plotted in green. We can see that the ratio between the PSD of the pressure signal and the PSD of the fluctuations produced by B1 thermal susceptibility is always greater than 30 dB except at the diurnal period. This means that the thermal susceptibility of the microbarometer will not significantly affect the pressure signal in comparison with the other sources of error (Marty et al. 2010) except at the diurnal period.

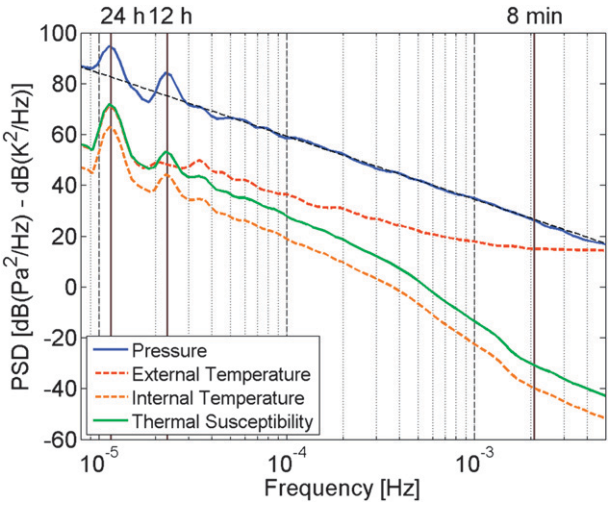

FIG. 6. PSD of the pressure signal recorded by the B1 measuring chain over 21 days (blue) and linear approximation of this PSD in the gravity wave–frequency band (dashed black). The PSD of the temperature recorded inside the sensor measurement cavity is represented in dashed orange and that recorded outside the measurement site B1 in dashed red. The green curve represents the PSD of the spurious fluctuations produced by the thermal susceptibility of the B1 microbarometer.

To evaluate the error produced by the sensor thermal susceptibility, we first characterized the averaged diurnal pressure oscillation recorded by each measuring chain using the superimposed epoch method (Panofsky and Brier 1958) on a diurnal time interval. We then selected the diurnal spectral complex components of the resulting signals. According to the fact that the maximum distance between the four microbarometers of each station (<1 km) is negligible compared to the dimension of the diurnal surface pressure perturbation produced by atmospheric tides, the four microbarometers of each station (A, B, and C) of the M2008 network should detect the same diurnal pressure fluctuation. However, we can see in Table 1 that the relative standard deviation (RSD) between the amplitude of the diurnal oscillations measured at the four measuring chains of each station can reach 17.4%. This confirms that the thermal susceptibility can significantly affect the pressure signal at the diurnal period.

In section 2b, we saw that the period of the expected eclipse signals ranged from 4 to 16 h, which is close to the diurnal period. To ensure identifying the pressure fluctuations produced by the passage of the solar eclipse

TABLE 1. Mean amplitude and RSD of the time-averaged diurnal pressure oscillation recorded by the four measuring chains of each station (A, B, and C) of the M2008 network without correction of pressure signals (none), with correction including the thermal susceptibilities provided by the manufacturer (correction 1), and with correction including the thermal susceptibilities evaluated in CEA's laboratories (correction 2).

Station	Correction type	Mean amplitude (Pa)	RSD (%)
A	None	113	3.96
	Correction 1	119	6.08
	Correction 2	120	2.91
B	None	105	1.66
	Correction 1	108	3.11
	Correction 2	107	1.63
C	None	106	17.4
	Correction 1	120	6.10
	Correction 2	122	2.33

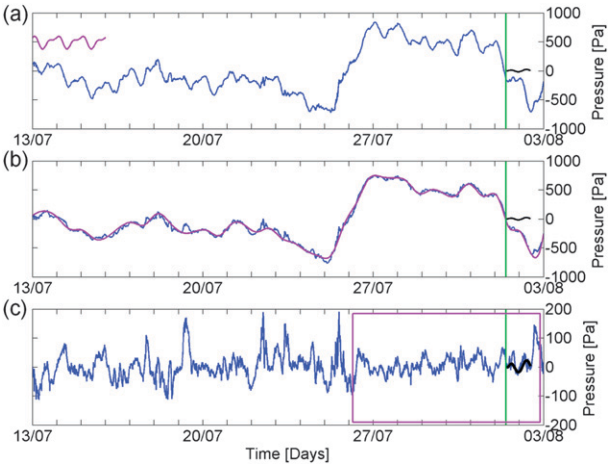

FIG. 7. (a) Pressure fluctuation signal recorded at the B1 measurement point (blue) and averaged diurnal and semidiurnal pressure oscillation (purple). (b) Pressure fluctuation signal subtracted from the averaged diurnal and semidiurnal pressure oscillation (blue) and cubic spline approximating large-scale pressure perturbations (purple). (c) Pressure signal subtracted from the cubic spline (blue). The purple rectangle represents the part of the signal analyzed within the time–frequency domain in Fig. 9. The eclipse signal produced from the model with the tropospheric source is plotted in black in all figures. Green vertical lines represent the time of the total solar eclipse.

and not some simultaneous fluctuations produced through temperature changes, we decided to compensate all the pressure signals from the influence of the temperature. To do so, we multiplied the temperature measurements recorded inside each microbarometer by the thermal susceptibility of the microbarometer and removed the resulting signal from the pressure signal. The thermal susceptibility is measured at −25° and +60°C during the manufacturing process, assuming that it is constant over this temperature range. To better estimate the thermal susceptibility of microbarometers, we decided to measure it in CEA's laboratories for 10 temperature steps ranging from +15° to +30°C. This temperature range covers values observed during the M2008 measurement campaign. The influence of the correction using these two estimations of the thermal susceptibility was characterized by calculating the RSD of the amplitude of the diurnal pressure oscillation recorded by the four microbarographs of each station (Table 1). We can see that the signal correction using the thermal susceptibility provided by the manufacturer (correction 1) modifies the diurnal oscillation amplitude but that the RSD remains important. On the contrary, the signal correction using the thermal susceptibility evaluated in CEA's laboratories (correction 2) allows an excellent correction of the pressure signals since the RSDs are lower than 2.9%. This value is highly satisfactory since the other sources of error such as the measuring chain instrumental noise can reach 3% (Marty et al. 2010). The difference between the two measurements of the thermal susceptibility probably results from the fact that the thermal susceptibility is not constant over the considered temperature ranges.

2) TIME–FREQUENCY ANALYSIS

The pressure signal recorded during 21 days by the B1 measuring chain is plotted in Fig. 7a (blue). It has been corrected from the sensor thermal susceptibility according to the discussion in section 4a(1). The synthetic signal obtained from the model with the tropospheric source (cf. section 2b) is overplotted in black to the right of the vertical green line. The amplitude of this signal is two orders of magnitude smaller than the maximum pressure fluctuations recorded by the B1 measuring chain. The synthetic signal corresponding to the stratospheric source is not shown since its amplitude is even smaller. Diurnal and semidiurnal oscillations can be clearly seen on the recorded pressure signal. As discussed in previous sections, these oscillations are produced by atmospheric tides and are in the same period range as the synthetic eclipse signals but with amplitude one or two orders of magnitude higher. It is therefore essential to remove these oscillations from the pressure signal to identify the pressure fluctuations produced by the passage of the total solar eclipse.

To do so, we consider that these diurnal and semidiurnal oscillations do not vary significantly over the duration of the measurement campaign. This approximation is especially valid for the semidiurnal oscillation, which mainly results from the daily heating of the stratospheric ozone layer. We then calculate the averaged tide amplitude by applying the superimposed epoch method (Panofsky and Brier 1958) on a diurnal time interval and by selecting the diurnal and semidiurnal

components of this signal. The averaged diurnal and semidiurnal pressure oscillations obtained with this method are plotted in purple on the left side of Fig. 7a. They are removed from the pressure signal in Fig. 7b (blue). In this resulting signal, large-amplitude pressure fluctuations produced by meteorological processes can still be seen. These fluctuations have periods exceeding 24 h and are not exactly in the same period range as the expected eclipse signals. However, they are very energetic and can potentially mask the waves produced by the eclipse depending on the signal processing method used. These fluctuations are therefore fitted with a cubic spline, which is then removed from the signal. The residual signal is plotted in blue in Fig. 7c.

At this stage, it seems that a pressure fluctuation with a similar waveform as the synthetic signal obtained corresponding to the tropospheric source (plotted in black) can be seen in the pressure signal. However, this fluctuation is still mixed in the middle of ambient pressure fluctuations. We therefore applied a wavelet transform to this signal using the Morlet wavelet with the nondimensional-frequency parameter $\omega_0 = 6$, which seems to be a reasonable compromise between the time and the frequency resolution (Torrence and Compo 1998). In Fig. 6, we can see that the power-law spectral index of the pressure fluctuation PSD (black dashed curve) is roughly constant in the gravity wave band. It is estimated to -2.48 with a logarithmic fit. To produce a scalogram that approximately ensures equal weight to all wavelet components within the full gravity wave–period band, the scalogram is divided by the function $f^{-2.48}$ (with f the frequency) before applying the wavelet transform. Figure 8 represents the scalogram of the pressure signal contained within the purple rectangle in Fig. 7c. The time of the total solar eclipse is indicated by the vertical green line. Note that the stations of the M2008 measurement campaign were uninstalled on 3 August 2008, thus no pressure records are available after this date.

3) TROPOSPHERIC RESPONSE

We can first observe that there is no significant energy detected in the 12–24-h-period range except after the passage of the solar eclipse. This shows that most of the energy produced by diurnal and semidiurnal atmospheric tides was successfully removed from the pressure signal. It also strongly suggests that the solar eclipse is the source of the pressure fluctuation observed in this bandwidth just after the passage of the solar eclipse. If we focus on the time–frequency characteristics of this pressure signal, we can see that its period increases from 8 to 14 h and that its maximum amplitude arrives about 20 h after the passage of the solar eclipse. These characteristics are close to those of the synthetic pressure signal related to the tropospheric source (Fig. 4). This signal is therefore likely to have been produced by the cooling of the troposphere during the total solar eclipse of the 1 August 2008.

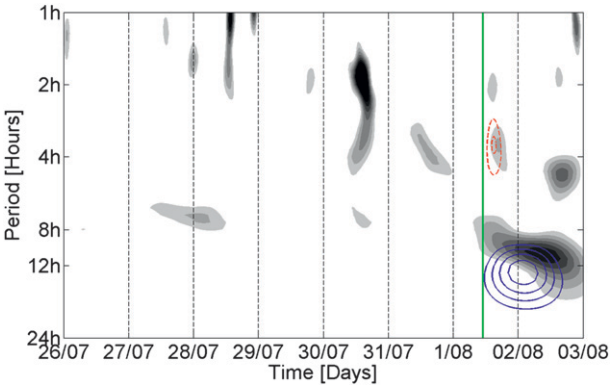

FIG. 8. Scalogram of the pressure signal recorded at the B1 measurement point between 26 Jul and 3 Aug 2010. The green vertical line represents the time of the total solar eclipse. The solid blue and dashed red contours respectively correspond to the scalograms of the synthetic pressure signals obtained from the model with the tropospheric and stratospheric source. The first (lowest) contour level is the same for both the recorded and the synthetic signals. Amplitudes of the synthetic troposphere and stratosphere are respectively multiplied by a factor of 3 and 20.

To better compare the time–frequency characteristics of the recorded and synthetic tropospheric signal, we also computed the scalogram of the synthetic signal (Fig. 8, solid blue contours). The amplitude of the synthetic tropospheric signal was multiplied by a factor of 3 in order to obtain comparable energy between the synthetic and observed signal. We can see that the period of the synthetic signal is slightly longer than that of the recorded signal. The maximum amplitude arrives also slightly earlier in the case of the synthetic signal. Given the approximations considered in the modeling of the source shape and intensity, these differences are not surprising. The fact that the amplitude of the synthetic signal is lower than that of the recorded signal is expected because the radiative effects of the cloud layers and of the ground surface were neglected in the simulation and a horizontally constant tropospheric absorption coefficient was chosen. Eckermann et al. (2007), who took into account a more complex tropospheric absorption coefficient, simulated ground pressure fluctuations that were slightly larger for the 2002 total solar eclipse (see section 2a). This probably means that we underestimated the amplitude of the tropospheric cooling in our simulation.

4) STRATOSPHERIC RESPONSE

If we now look at other period ranges, we see several other pressure fluctuations arriving just after the passage of the solar eclipse. It is difficult to determine whether they are produced by the passage of the solar eclipse since pressure fluctuations with similar time–frequency characteristics can be observed at other times. However, we can see a low-amplitude pressure fluctuation with a 4–5-h period occurring just after the passage of the solar eclipse. Looking at the pressure signal produced from the model with the stratospheric source (Fig. 4), we can see that the maximum amplitude is also reached 2–3 h after the passage of the solar eclipse and that its period is about 5 h at this time. The scalogram of the synthetic stratospheric pressure signal is plotted in dashed red contours. The amplitude of the synthetic stratospheric signal was multiplied by a factor of 20 in order to obtain comparable energy between the synthetic and observed signal. It can be seen that the time-frequency characteristics of the synthetic signal are close to those of the recorded signal. This suggests that the pressure fluctuation could have been produced by the cooling of the stratosphere during the passage of the 1 August 2008 total solar eclipse.

There is nevertheless a factor of 20 between the amplitude of the synthetic and the observed signals. The modeling of the atmospheric response to the cooling of the ozone layer during the 2008 solar eclipse (section 2b) predicts temperature fluctuations with a maximum amplitude of about 1 K at 50-km altitude. This result is in agreement with Eckermann et al. (2007) who obtained similar values for the 2002 total solar eclipse with a prototype high-altitude global numerical weather prediction model. However, Eckermann et al. (2007) pointed out that several rocket soundings reported temperature decreases of 5–12 K at 50–60-km altitude during solar eclipses (Ballard et al. 1969; Quiroz and Henry 1973; Randhawa 1974; Schmidlin and Olsen 1984). It is thus possible that the amplitude of the stratospheric thermal forcing term was not properly estimated in our model. This amplitude discrepancy calls for future investigation and model improvements.

b. IMS pressure measurements

Identical pressure fluctuations were detected by all the microbarometers of the M2008 measurement campaign. This result was expected since the microbarometers are relatively close to one another compared to the dimension of the ground pressure perturbation. We therefore looked at the pressure signal detected by the four IMS stations closest to the total eclipse path. To extract the eclipse signal, we corrected the pressure signals from the sensor transfer function (Marty et al. 2010) and applied the same method described in section 4a(2). The pressure fluctuations produced by atmospheric tides and synoptic disturbances were therefore removed from the pressure signals. Figure 9 represents the scalogram obtained for the four IMS infrasound stations I18DK, I31KZ, I46RU, and I34MN. The scalograms of the corresponding synthetic tropospheric signals are overplotted in blue contour. Here, the amplitude of the synthetic tropospheric signals was multiplied by a factor of 4.

Waves with periods of 12–16 h can clearly be seen just after the passage of the solar eclipse at the I18DK, I31KZ, and I34MN stations. It is worth noting that there is no other significant energy detected in the 6–24-h-period band during the entire time period. This strongly suggests that there is a link between the passage of the solar eclipse and the observed energy. Moreover, we can see that at these three stations, the time–frequency characteristics of the synthetic signals are very similar to those of the observed signals. As for the M2008 data, the observed amplitudes are slightly lower but this is not surprising according to the approximation used in the simulation and discussed in section 4a(2). A wave with time–frequency characteristics similar to those of the tropospheric synthetic signal was also observed at I46RU. However, this wave arrives too late (2 days later) to have been produced by the cooling of the troposphere during the 2008 solar eclipse. This shows that other sporadic atmospheric phenomena can produce waves with similar characteristics as those observed after the passage of the solar eclipse at other stations. A 4-h-period pressure signal with similar characteristics as that of the stratospheric synthetic signal was also observed at the I18DK station just after the passage of the solar eclipse. However, the observed amplitude is 30 times greater than that of the synthetic signal. Since other pressure signals are also observed in the same period range at other times, there is no evidence that this signal was produced by the passage of the solar eclipse.

5. Conclusions

In this article, we used the linear spectral numerical model described by (Marty et al. 2010) to estimate the surface atmospheric pressure perturbation produced by the cooling of the atmosphere during the passage of a solar eclipse. While the cooling of both the troposphere and stratosphere can produce detectable pressure fluctuations at Earth's surface, it was found that the tropospheric cooling is much more likely to be the predominant source. We then estimated the pressure fluctuations produced by the passage of the 1 August 2008

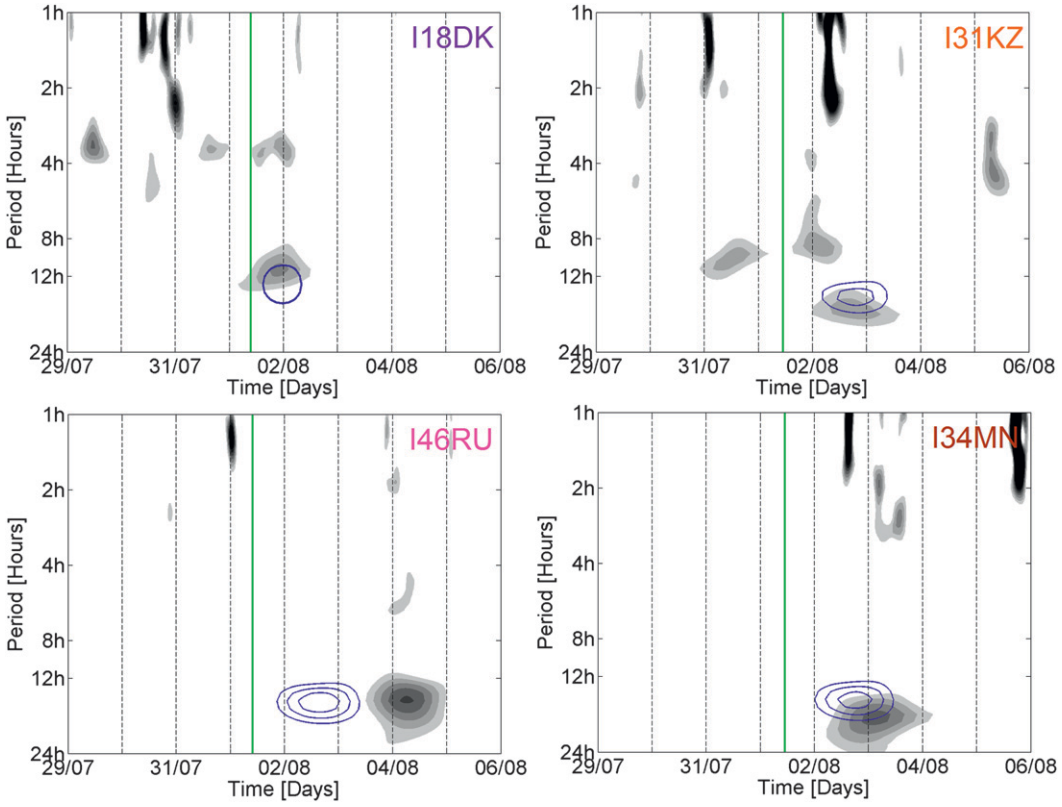

FIG. 9. Scalogram of the pressure signals recorded at the four closest certified IMS infrasound stations to the total eclipse path: I18DK, I31KZ, I46RU, and I34MN. Green vertical lines represent the time of the total solar eclipse at each station. The solid blue contours correspond to the scalograms of the synthetic pressure signals obtained from the model with the tropospheric source. The first contour level is the same for both the recorded and the synthetic signals but the amplitude of the synthetic signals was multiplied by a factor of 4.

solar eclipse at the position of different microbarograph networks. We showed that the amplitude of the simulated pressure fluctuations was rather low compared to that of ambient pressure fluctuations. This is especially true for the pressure fluctuations produced by the tropospheric source as their period is in the same frequency band as the pressure oscillations produced by atmospheric tides. A series of filtering operations was therefore required in order to identify the pressure fluctuations produced by the passage of the solar eclipse. The averaged pressure oscillations produced by atmospheric tides were first characterized and removed from all pressure signals. The energetic meteorological disturbances produced at periods longer than 24 h were then filtered out. The resultant pressure signals showed long-period pressure fluctuations just after the passage of the solar eclipse at all the stations of the M2008 measurement campaign and at most IMS infrasound stations located close to the total eclipse path. The time–frequency characteristics of these identified pressure fluctuations (estimated through the Morlet wavelet transform) are similar to that obtained from the model with the tropospheric source. This strongly suggests that these waves were produced by the passage of the total solar eclipse of 1 August 2008. Waves with similar time-frequency characteristics as synthetic pressure fluctuations obtained with the stratospheric source were also observed. Such waves could therefore have been produced by the cooling of the ozone layer during the passage of the solar eclipse. However, the amplitude of these waves was too high to be explained by the simulations.

Figure 10 shows a summary of the observations from several experiments after the passage of solar eclipses. The observations are presented as a function of the period of the observed waves and of the distance between the stations and the central line of the solar eclipse. This figure points out that the detection of low-frequency waves at such a number of stations constitutes, to our knowledge, a unique result. The lack of previous detections might be due to several reasons. First, the record of such fluctuations requires the use of high dynamic range pressure sensors whose response is well

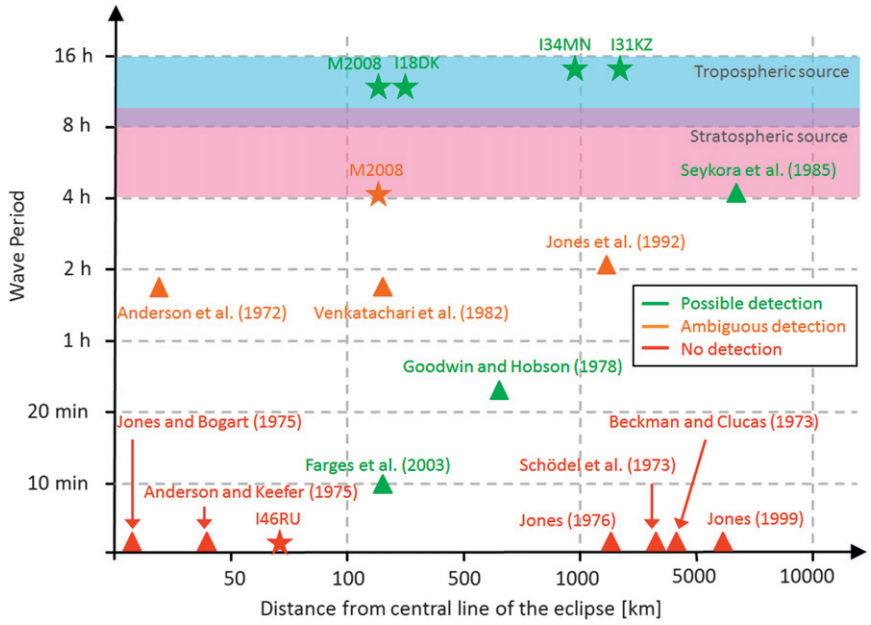

FIG. 10. Summary of the observations from several experiments after the passage of solar eclipses (triangles for observations from previous experiments and stars for observations shown in this paper). The observations are represented as a function of the period of the observed waves and of the distance of the stations from the central line of the total eclipse path.

understood and mastered. Second, the pressure sensors need to detect pressure fluctuations in the entire frequency range and not only the highest-frequency part of the gravity wave spectrum. Third, to our knowledge, apart from Chimonas (1970), no pressure waveforms were estimated for the ground level, increasing the difficulty to distinguish waves produced by the eclipse from other fluctuations. Finally, the waves produced by the passage of a solar eclipse are in a frequency band highly disturbed by atmospheric tides and meteorological phenomena and their extraction requires the use of specific signal processing methods.

Since previous authors (Anderson et al. 1972; Goodwin and Hobson 1978; Farges et al. 2003) reported gravity waves produced by solar eclipses with period ranging from 10 to 90 min, we also looked for pressure signals in this period range. Such signals were identified at the stations A, B, and C of the temporary network M2008, but there was no particular link between these pressure fluctuations and the passage of the solar eclipse. As discussed in the present paper, such waves can be produced by the radiative cooling of smaller-size sources such as cloud layers or water vapor inhomogeneities (Chimonas 1973). To determine whether these waves could have been produced by the passage of the 1 August 2008 solar eclipse, additional modeling efforts, including water vapor profiles and the position of clouds layers, would be necessary. Finally, we would like to point out that the IMS infrasound network is a valuable source of data for analyzing surface pressure fluctuations produced by solar eclipses. Total solar eclipses occur indeed on average once a year at Earth's surface and the first IMS infrasound stations have been installed more than 10 years ago with now 45 certified stations. As seen in Fig. 10, the IMS infrasound network provides a great range of simultaneous observations compared to temporary or isolated sensors. The analysis of IMS infrasound data for several solar eclipses could therefore further demonstrate that the passage of the moon shadow regularly produces detectable atmospheric pressure fluctuations at Earth's surface.

Acknowledgments. The views expressed herein are those of the authors and do not necessarily reflect the views of the CTBTO Preparatory Commission. This research project was funded by the CEA, DAM, DIF. It would not have been possible without the support of the Research Center of Astronomy and Geophysics of the Mongolian Academy of Sciences. The authors particularly wish to express their gratitude to Prof. Ph.D. S. Demberel for coordinating the Mongolia 2008 measurement campaign and to Mr. B. Battulga and Ch. Bayarsaikhan for their on-site engineering and logistical assistance. Deepest gratitude is also due to Mr. S. Zagdsuren and his team at the Hovd local seismic station for their most valuable help.

REFERENCES

Anderson, R. C., and D. R. Keefer, 1975: Observation of temperature and pressure changes during 30 June 1973 solar eclipse. *J. Atmos. Sci.,* **32,** 228–231.

——, ——, and O. E. Myers, 1972: Atmospheric-pressure and temperature changes during 7 March 1970 solar eclipse. *J. Atmos. Sci.,* **29,** 583–587.

Ballard, H. N., R. Valenzuela, M. Izquierdo, J. S. Randhawa, R. Morla, and J. F. Bettle, 1969: Solar eclipse: Temperature, wind, and ozone in stratosphere. *J. Geophys. Res.,* **74,** 711–712.

Beckman, J. E., and J. I. Clucas, 1973: Search for atmospheric gravity waves induced by the eclipse of June 30, 1973. *Nature,* **246,** 412–413.

Chapman, S., and K. C. Westfold, 1956: A comparison of the annual mean solar and lunar atmospheric tides in barometric pressure as regards their world-wide distribution of amplitude and phase. *J. Atmos. Terr. Phys.,* **8,** 1–23.

Chimonas, G., 1970: Internal gravity-wave motions induced in the Earth's atmosphere by a solar eclipse. *J. Geophys. Res.,* **75,** 5545–5551.

——, 1973: Lamb waves generated by 1970 solar eclipse. *Planet. Space Sci.,* **21,** 1843–1854.

Dai, A., and J. Wang, 1999: Diurnal and semidiurnal tides in global surface pressure fields. *J. Atmos. Sci.,* **56,** 3874–3891.

DASE, 1998: Microbarometer MB2000 technical manual. CEA, 64 pp.

Eaton, F. D., J. R. Hines, W. H. Hatch, R. M. Cionco, J. Byers, D. Garvey, and D. R. Miller, 1997: Solar eclipse effects observed in the planetary boundary layer over a desert. *Bound.-Layer Meteor.,* **83,** 331–346.

Eckermann, S. D., D. Broutman, M. T. Stollberg, J. Ma, J. P. McCormack, and T. F. Hogan, 2007: Atmospheric effects of the total solar eclipse of 4 December 2002 simulated with a high-altitude global model. *J. Geophys. Res.,* **112,** D14105, doi:10.1029/2006JD007880.

Espenak, F., and J. Anderson, 2001: Total solar eclipse of 2002 December 04. NASA Tech. Paper NASA/TP-2001-209990, 77 pp.

——, and ——, 2007: Total solar eclipse of 2008 August 01. NASA Tech. Paper NASA/TP-2007-77, 68 pp.

Farges, T., A. Le Pichon, E. Blanc, S. Perez, and B. Alcoverro, 2003: Response of the lower atmosphere and the ionosphere to the eclipse of August 11, 1999. *J. Atmos. Sol. Terr. Phys.,* **65,** 717–726.

Fritts, D. C., and Z. G. Luo, 1993: Gravity-wave forcing in the middle atmosphere due to reduced ozone heating during a solar eclipse. *J. Geophys. Res.,* **98** (D2), 3011–3021.

——, and M. J. Alexander, 2003: Gravity wave dynamics and effects in the middle atmosphere. *Rev. Geophys.,* **41,** 1003, doi:10.1029/2001RG000106.

Goodwin, G. L., and G. J. Hobson, 1978: Atmospheric gravity waves generated during a solar eclipse. *Nature,* **275,** 109–111.

Jones, B. W., 1976: Search for lamb waves generated by solar eclipse of 11 May 1975. *J. Atmos. Sci.,* **33,** 1820–1823.

——, 1999: A search for atmospheric pressure waves from the total solar eclipse of 9 March 1997. *J. Atmos. Sol. Terr. Phys.,* **61,** 1017–1024.

——, and R. S. Bogart, 1975: Eclipse induced atmospheric gravity waves. *J. Atmos. Terr. Phys.,* **37,** 1223–1226.

——, G. J. Miseldine, and R. J. A. Lambourne, 1992: A possible atmospheric pressure wave from the total solar eclipse of 22 July 1990. *J. Atmos. Terr. Phys.,* **54,** 113–115.

Marty, J., and F. Dalaudier, 2010: Linear spectral numerical model for internal gravity wave propagation. *J. Atmos. Sci.,* **67,** 1632–1642.

——, D. Ponceau, and F. Dalaudier, 2010: Using the international monitoring system infrasound network to study gravity waves. *Geophys. Res. Lett.,* **37,** L19802, doi:10.1029/2010GL044181.

Panofsky, H. A., and G. W. Brier, 1958: *Some Applications of Statistics to Meteorology.* The Pennsylvania State University, 224 pp.

Ponceau, D., and L. Bosca, 2010: Low-noise broadband microbarometers. *Infrasound Monitoring for Atmospheric Studies,* A. Le Pichon, E. Blanc, and A. Hauchecorne, Eds., Springer, 119–140.

Quiroz, R. S., and R. M. Henry, 1973: Stratospheric cooling and perturbation of meridional flow during solar eclipse of 7 March 1970. *J. Atmos. Sci.,* **30,** 480–488.

Randhawa, J. S., 1974: Partial solar eclipse effects on temperature and wind in an equatorial atmosphere. *J. Geophys. Res.,* **79,** 5052–5054.

Schmidlin, F. J., and R. O. Olsen, 1984: Modification of the stratomesospheric temperature and wind structure resulting from the 26 February 1979 solar eclipse. *J. Atmos. Sol. Terr. Phys.,* **46,** 273–280.

Schödel, J. P., J. Klosterm, and J. Rottger, 1973: Atmospheric gravity wave observations after solar eclipse of June 30, 1973. *Nature,* **245,** 87–88.

Seykora, E. J., A. Bhatnagar, R. M. Jain, and J. L. Streete, 1985: Evidence of atmospheric gravity-waves produced during the 11 June 1983 total solar eclipse. *Nature,* **313,** 124–125.

Simpson, G. C., 1918: The twelve-hourly barometer oscillation. *Quart. J. Roy. Meteor. Soc.,* **44,** 1–19.

Torrence, C., and G. P. Compo, 1998: A practical guide to wavelet analysis. *Bull. Amer. Meteor. Soc.,* **79,** 61–78.

Venkatachari, R., A. K. Saha, C. V. Subrahmanyam, and S. K. Chatterjee, 1982: Evidence of atmospheric gravity waves in the wake of the eclipse shadow. *Proc. Indian Natl. Sci. Acad.,* **48,** 370–374.

——, V. K. Vohra, and V. P. Sachdeva, 1996: Observations on infrasonic pressure variations during the total solar eclipse of 24 Oct. 1995. *Indian J. Radio Space Phys.,* **25,** 61–63.